An Improved Model of Stacked Short Time Fourier Transform and SqueezeNet Using Golden Jackal Algorithm for Rolling Bearing Fault Detection

Thomas JOSEPH *
Department of Mechanical Engineering, Jyothi Engineering College, Thrissur, APJ Abdul Kalam Technological University, Thiruvananthapuram, Kerala, India, tjk4411@gmail.com

Sudeep ULLATTIL
Department of Mechanical Engineering, NSS College of Engineering, Palakkad, APJ Abdul Kalam Technological University, Thiruvananthapuram, Kerala, India, usudeep@gmail.com

Keerthi Krishnan K
Department of Electronics and Communication Engineering, NSS College of Engineering, Palakkad, APJ Abdul Kalam Technological University, Thiruvananthapuram, Kerala, India, keerthi.ack@gmail.com

* Author to whom correspondence should be addressed

Abstract: - Rolling bearings are critical components in rotating machinery, and their fault detection is essential for ensuring the machinery's risk-free operation. Fault detection techniques equipped with deep learning (DL) models have been in focus recently. This work presents an efficient rolling bearing fault detection model using the Stacked Short Time Fourier Transform (S-STFT) and an enhanced SqueezeNet model. The enhanced SqueezeNet is the integration of SqueezeNet and the golden jackal algorithm (GJA). Initially, the S-STFT is utilized for converting the vibration signals into time-frequency images. Then, the images are fed to the enhanced SqueezeNet for efficient feature extraction and fault detection. For verifying the efficiency of the suggested fault detection model, two datasets are considered, and achieved accuracies of 99.65% on the CWRU and 99.71% on the test rig dataset, respectively.

Keywords: - Fault detection, Rolling bearings, Short Time Fourier Transform, enhanced SqueezeNet.

1. INTRODUCTION

Rolling bearings are extensively utilized in industries and are one of the most prevalent parts in rotating machinery. Their proper functioning is crucial for the continuous and secure operation of mechanical equipment, making proactive fault diagnosis essential [1]. Recently, various fault detection approaches have been proposed for rolling bearings [2]. After prolonged operation under complex conditions, these bearings are susceptible to various faults, including corrosion, rolling body deformation, cracks, and wear. Faults in bearings generally occur due to a combination of factors like fatigue, wear, improper lubrication, and contamination. Damaged rolling bearings can lead to significant accidents in practical engineering systems, resulting in substantial safety concerns and economic losses [3].

Conventional data-driven fault diagnosis techniques rely on the extraction of meaningful fault features from acquired signals. Conventional feature extraction models like the Fourier transform (FT), empirical model decomposition (EMD), and wavelet transform (WT) have been utilized in the existing works [4]. Many machine learning (ML) techniques have been investigated in the field of fault detection. Some of the fault diagnosis methods include Support Vector Machines (SVMs), Decision Trees, and Linear Regression analysis [5] SVMs can classify faults by utilizing extracted features to differentiate between normal and defective bearings [6]. However, these techniques rely on prior information about fault features and the involvement of trained manpower, which is considered a hindrance in automation.

Therefore, researchers have attempted the integrate deep learning (DL) with signal processing techniques to address this challenge. By pre-processing fault signals with appropriate algorithms, they can eliminate redundant information, allowing key fault characteristics to be captured more effectively and automatically [7]. This reduces the

complexity of building diagnostic models. Both conventional intelligent diagnosis methods and DL based approaches have significantly advanced in bearing fault diagnosis. However, most of the current research relies on supervised learning, which necessitates a substantial amount of labeled data for training [8]. In real-world scenarios, the process of manually labelling a large number of samples is both labor-intensive and time-consuming, demanding considerable expertise. As a consequence, when a significant portion of the dataset lacks labeled data, it presents challenges for supervised learning methods to effectively perform fault diagnosis [9-12].

Although the DL approaches are increasingly being applied in rolling bearing fault diagnosis with better outcomes, they still have certain limitations. As the number of hidden layers increases, some DL approaches need high computation time and cost. Conventional approaches also have their drawbacks, such as poor effectiveness, a lack of robustness, time consumption, and manual processes. Therefore, it is essential to propose an improved method that offers high efficiency, low resource requirements, and high speed in computation. Hence, this work aims to design a robust method for fault detection in rolling bearings. The major steps in this study are:

- Transforming the 1D vibration signals to time and frequency images for input to the STFT-enhanced SqueezeNet.
- Capturing the fault features and highlighting distinct properties of the fault.
- Introducing the golden jackal algorithm (GJA) for optimizing the performance of enhanced SqueezeNet and enhancing the accuracy.

The rest of the work is organized as follows: related literature is provided in Section 2, the proposed methodology is provided in Section 3; Section 4 provides the analysis of results, and Section 5 presents the conclusion.

.

2. RELATED WORKS

The fault detection in rolling bearings using the optimum ensemble deep transfer model (OE-DTM) was illustrated in [13]. Various kernel maximum mean discrepancies were utilized for constructing the DTM. Later, the particle swarm optimizer (PSO) was used for assigning weights to the DTM, and an accuracy value of 84.2% was achieved on the CWRU dataset. A structural similarity GAN (SS-GAN) and improved MobileNetv3 CNN (IM-CNN) for fault diagnosis in rolling bearings was presented in [14]. The wavelet transform images are generated, and the samples are generated using SS-GAN, and IM-CNN is used for extracting the essential features. For increasing the classification outcomes, the IM-CNN considered the self-focusing module. Fault detection in rolling bearings using EMD and symmetrized dot pattern (SDP) was proposed in [15]. Initially, the EMD was used for decomposing the signals into various intrinsic mode functions (IMFs). The initial 5-IMFs were transformed into five symmetrical snowflake images. The feature matrices and the adaptive Manhattan distance were computed, and the accuracy value attained was 97.5% for IMF-1. A hybridized multi-modal based DL model for fault diagnosis in rolling bearings was demonstrated in [16]. In this work, the time series features are converted to greyscale images, which are classified using CNN and DBN. The experiment was carried out by varying the CNN-1, 2, and 3, and DBN-1, 2, and 3 were considered, and four types of faults were identified; the AUC value achieved was 0.98.

A signal-to-image mapping (STIM) of rolling bearings signals for fault diagnosis was suggested in [17]. At first, the data augmentation was increasing the data samples. Then, the STIM was used for converting the 1D signal to 2D grayscale images. At last, the CNN was used for extracting the features and analyzing the classification of faults. Accuracy values achieved were 98.7% (CWRU) and 99.8% (rolling element bearing) datasets. An overlapped group sparse approach, which develops weighting terms by verifying the prominent signal features, was proposed in [18]. The sparse optimization model was solved using convex optimization and the features were extracted. To address the challenge of identifying multi-scale features, the CNN was presented.

Local mean decomposition (LMD) with multiple scale symbolic dynamical information entropy (MSDE) for fault diagnosis in rolling bearing was also suggested [19]. Initially, the LMD was used for extracting the original signal's information. Then, the entropy values were combined with LMD and MSDE was used for extracting the feature sets. These features were fed to the affinity clustering for identifying the faults. A PReLU based DBN optimized model for fault identification in rolling bearings was proposed in [20]. The features were reduced by the principal component analysis (PCA), and the faults were classified by the PReLU. Here, the PSO was used for updating the weights of the DBN, and the accuracy value achieved was 98.4%. Faults in rolling bearings were identified by vibration and shock impulses [21]. Here, the Fast Fourier transform (FFT) was used for extracting the shock impulses. The literature surveyed reveals that DL approaches have been extensively used in rolling bearing fault detection. However, as the approach's complexity and the hyperparameters grow exponentially, managing them becomes increasingly challenging.

This work presents a GJA to automatically adjust the hyper-parameters, while the SqueezeNet extensively extracts the features and classifies the faults.

3. PROPOSED METHODOLOGY

The process begins with decomposing the rolling bearing signals into variational mode decomposition (VMD) modes. Each of the VMD modes is denoised using the wavelet denoising method with adaptive thresholding, after which the STFT of the denoised modes is computed. Finally, the STFT of modes is stacked in the time domain to form the S-STFT. These images are subsequently fed into the enhanced SqueezeNet for feature extraction and classification. Figure 1 illustrates the pipeline of the suggested fault diagnosis approach with respect to the S-STFT and enhanced SqueezeNet.

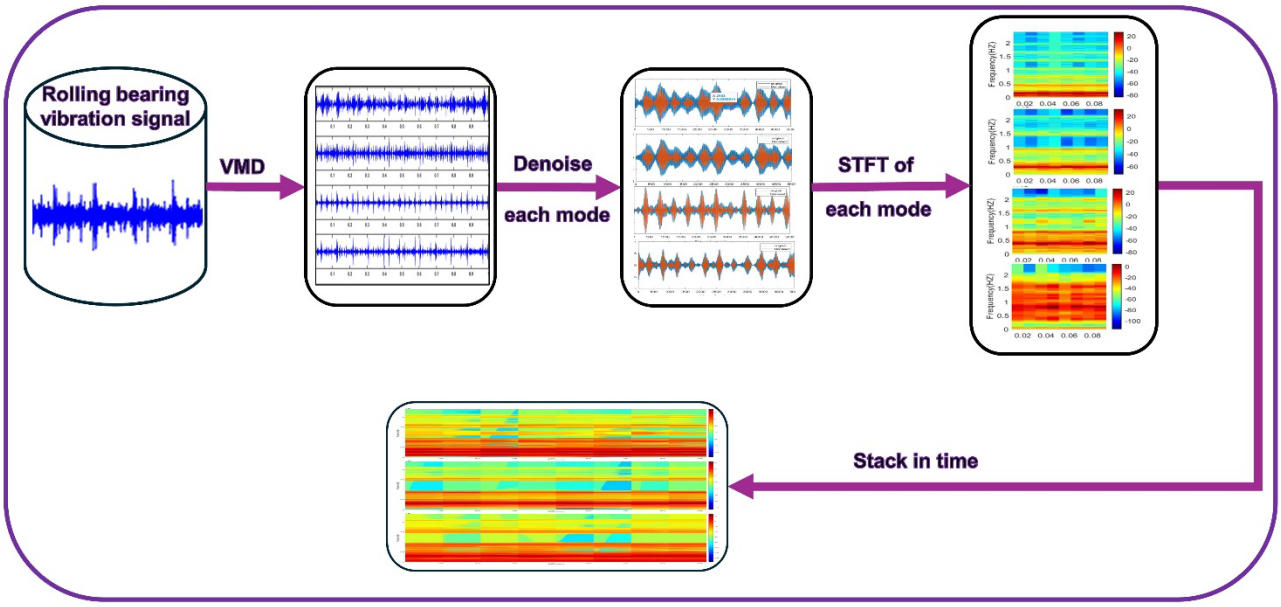

Figure 1. Flow diagram of the proposed fault diagnosis approach.

During the pre-processing phase, the vibrating signals are transformed to time-frequency images, and Z-score normalization is used to normalize the data.

$$X_k = \frac{x_k - \alpha}{\sigma} \quad (1)$$

where X_k, x_k, α and σ are the normalized data, S-STFT, mean, and standard deviation. After normalization, the training data is fed into the enhanced SqueezeNet model, which reduces the loss function. Initially, the obtained signals are divided by random sampling. To prevent the leakage of data, it is ensured that there is no overlap in the samples. Both datasets are split as 70% (training), 10% (validation), and 20% (testing) for the experimental process.

3.1. Conversion of the vibration signal to an image

STFT is a method used for combined time and frequency analysis of signals, which transforms 1D fault vibrating signals into 2D images that encompass both time and frequency domain information. The core principle of STFT involves using a constant windowing-length term to divide time domain signals, and then applying the FT to the segmented portions to obtain local spectra for small time intervals around each time t. By moving this constant windowing length across the overall period, a series of local spectra for every period is produced. Thus, STFT is represented as a 2D term of time and frequency, and it is computed as:

$$STFT\{z(t)\}(t,w) = \int_{-\infty}^{\infty} z(\alpha) f(\alpha - t) e^{-kwt} \quad (2)$$

where k is the imaginary part, $z(t)$ is the signal of the time domain, α and w are the shift in time and frequency, and $f(\alpha - t)$ is the window function. The window function considered is the Hamming window. The spectrum is measured as:

$$|STFT\{z(t)\}(t,w)|^2 = \left| \int_{-\infty}^{\infty} z(\alpha) f(\alpha - t) e^{-kwt^2} \right| \quad (3)$$

The window length term M_w shows the spectrum's time and frequency. A large $M_w$offers high frequency resolution after the FT, but time resolution is lower. Therefore, to achieve optimal analysis, the M_w should be selected appropriately based on the specific signals being analyzed. The time resolution is computed as:

$$T = \left[\frac{M_z - M_0}{M_w - M_0}\right] \quad (4)$$

where $M_z$is the signal's length to be pre-processed and M_0 is the overlapping length. Moreover, the resolution frequency is given as:

$$F = \begin{cases} M_w/2 + 1, & when\ M_w is\ even \\ (M_w/2 + 1)/2, & when\ M_w is\ odd \end{cases} \quad (5)$$

A logical determination in the time as well as frequency domains can enhance the visibility of fault signals and mitigate noise interference.

3.2 Fault classification

After the image conversion process, the time-frequency images are provided as input to the proposed enhanced SqueezeNet [22] for feature extraction and classification. SqueezeNet is a compact DL model that has been applied effectively in the rolling bearing fault detection model [23]. Its design aims to achieve high accuracy with fewer parameters compared to conventional CNNs. In the context of rolling bearing fault detection, SqueezeNet's efficiency allows for faster inference times and reduced computational load while maintaining competitive performance in accurately identifying faults based on vibration signals.

The enhanced SqueezeNet model is utilized for deriving the optimum feature vector set, with hyperparameters fine-tuned by the GJA. As shown in Figure 2, the enhanced SqueezeNet begins with the convolutional layer (conv1) and gradually increases the number of filters in each fire module throughout the network. The architecture employs max pooling having a stride2 following the conv1, fire4, fire8, and conv10 layers. There are 1 × 1 filters $(a_1 \times 1)$ in the squeeze layer, 3 × 3 filters $(b_3 \times 3)$and 1 × 1 filters $(b_1 \times 1)$ in the expanded layer in the fire layer. Each Fire layer contains 24 dimensional hyperparameters across 8 modules. For the j^{th} layer, the expanded filter is given as:

$$b_j = b_{j1} \times 1 + b_{j3} \times 3 = F + \left(J \times \left\lfloor \frac{j}{N} \right\rfloor\right) \quad (6)$$

where *F* is the total expanded filters in the first fire layer, *N* is the total fire layers, and the expanding filters are incremented by *J*.

Moreover, a bypass layer is integrated for mitigating the bottleneck that occurs due to the squeeze layers. But the challenge arises because the number of inputs of the Fire layer differs from the total outputs, making the element-wise addition infeasible. To address this, a complex bypass is defined as a bypass incorporating a 1 × 1 conv layer by the total filters, which makes the total outputs is equal. This approach enables the layer for learning a residual connection of input and output while simultaneously achieving a top conv layer enriched with semantic information. Finally, the SoftMax layer is used for identifying the fault types.

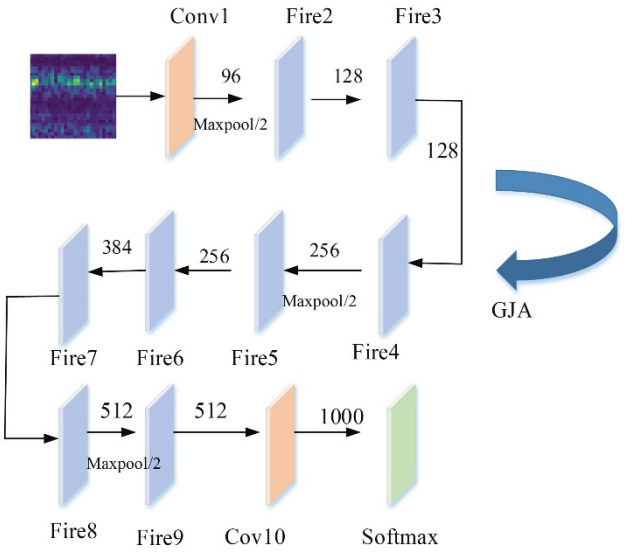

Figure 2. Structure of the enhanced SqueezeNet.

$$p(y_j = s|x_j) = \frac{e^{zs}}{\sum_k e^{zk}} \quad (7)$$

where $p(y_j = s|x_j)$ is the probability of the input x_j is categorized as a class s and zs is the output for class k. The loss function considered is cross-entropy, and it is given as:

$$Loss(\theta) = -\frac{1}{M} 1\{y_j = c\} log\ p\ (y_j = s|x_j; \theta) \quad (8)$$

where *M* is the overall training sample.

Further, to enhance the accuracy of the faults classification, the hyper-parameters like learning rate, dropout, and size of the batch are optimized by the metaheuristic optimization golden jackal algorithm (GJA) by considering the accuracy as the fitness function.

$$Fitness = Maximize(Accuracy) \quad (9)$$

GJA is a metaheuristic optimization that portrays the hunting strategy of golden jackals (GJ) in nature. Its hunting strategy consists of three phases: approach and search for prey, confuse and surround the prey, and finally, motion end and swoop on the prey. At the stage of initialization, a matrix of prey positions s $(P(0))$ is randomly generated by:

$$P(0) = \begin{bmatrix} W_{1,1} & W_{1,2} & \cdots & W_{1,dim} \\ W_{2,1} & W_{2,2} & \cdots & W_{2,dim} \\ \vdots & & \ddots & \vdots \\ W_{pop,1} & W_{pop,2} & \cdots & W_{pop,dim}[] \end{bmatrix} \quad (10)$$

where pop and dim are the prey's population and dimension. $A_s$is the prey's escaping energy, and it is given as:

$$A_s = A_1 A_0 \quad (11)$$

where $A_1$and $A_0$are the prey's decreasing energy and initial energy. The value of A_1 is computed by:

$$A_1 = b_1\left(1 - \frac{iter}{max\_iter}\right) \quad (12)$$

where $b_1$is the random number, $iter$and max_iter are the iteration and maximum iteration. When $|A_s| > 1$, the hunting of GJ is given as:

$$W_1(iter) = W_M(iter) - \\ -A_s|W_M(iter) - r \times P(iter)| \quad (13)$$

$$W_2(iter) = W_{FM}(iter) - \\ -A_s|W_{FM}(iter) - r \times P(iter)| \quad (14)$$

where $W_1(iter)$ and $W_2(iter)$ are the updated versions of male and female GJ; $W_M(iter)$ and $W_{FM}(iter)$ are the male and female places. $r$is the random number, and it is computed by Levy's flight.

$$LF = \frac{0.01 \times v \times \alpha}{u^{(1/\sigma)}} \quad (15)$$

$$\alpha = \left[\frac{\Gamma(1+\sigma)\, sin\frac{\pi\sigma}{2}}{\Gamma\left(\frac{1+\sigma}{2}\right)\sigma(2\sigma-1)}\right]^{1/\sigma} \quad (16)$$

where v and u are the randomized numbers. σ is set as 1.5. $P(iter)$ is the prey vector, and it is computed as:

$$P(iter) = |W_M(iter) - r \times P(iter)| \quad (17)$$

While the prey is exhausted from the chase, the A_s decreases. When $|A_s| \leq 1$, the surrounding GJ begin to devour the prey, a scenario described as:

$$W_1(iter) = W_M(iter) - \\ -A_s \times r \times W(iter) - P(iter) \quad (18)$$

$$W_1(iter) = W_{FM}(iter) - \\ -A_s \times r \times W(iter) - P(iter) \quad (19)$$

The value of the $P(W(iter+1))$ is computed by means of the $W_1(iter)$ and $W_2(iter)$

$$P(X(iter+1)) = \frac{W_1(iter) + W_2(iter)}{2} \quad (20)$$

Algorithm 1 presents the pseudocode of the GJA for updating the hyper-parameters of the SqueezeNet.

Table 1. Pseudocode of the GJA.

Algorithm 1: Pseudocode of the GJA
Input: Learning rate, dropout, size of the batch, iterations, and population size **Output:** Optimal value Initialize the position of the prey in a randomized manner Choose the best prey Determine the fitness using Equation (10) while $(t < max\_iter)$ do **for** every prey Update the $A_s$by Equations by (12) and (13) Update the r by Equations by (15) and (16) **if**$|A_s| > 1$ Update the prey's position by Equations by (14), (15) and (20) **else** $|A_s| \leq 1$ Update the prey's position by Equations by (18), (19) and (20) **End** **End** **end** $t = t + 1$ **End**

4. RESULTS AND DISCUSSION

To demonstrate the suggested fault detection model, experiments are conducted on two standard rolling bearing datasets using MATLAB. The experiments are run on a computer with 16 GB of RAM and 4 GB of VRAM. Table 2 presents the hyper-parameters of the proposed enhanced SqueezeNet.

Table 2. Hyper-parameters.

Hyper-parameters	Values
Size of batch	32
Learning rate	0.001
Epochs	100
Optimizer	GJA
Population size	20
Iterations	50

4.1. Datasets

Dataset 1 is Case Western Reserve University (CWRU) [24] Bearing Dataset, which is available in the public domain. Experimental data were gathered through controlled experiments involving bearings. The key elements involved in these experiments were an accelerometer, bearings, an electric motor, a torque transducer, and a dynamometer. A torque transducer is used for measuring the torque applied to a rotating system. To induce faults in the bearings, electric-discharge machining was employed. Defects were intentionally introduced at various locations, including the normal (NO), inner race (IR), outer race (OR), and rolling elements (RE), with fault size ranging from 0.007 inches to 0.0.021 inches. For the testing phase, defective bearings in the test motor were replaced, and vibration data was recorded across a range of motor loads, spanning from 0 to 3 horsepower (1797 to 1720 revolutions per minute (RPM)).

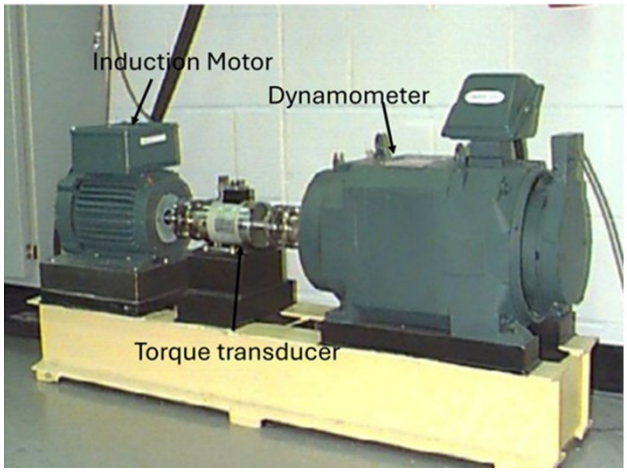

Figure 3. The experimental setup of the CWRU dataset.

Dataset 2 is a test rig dataset that has three classes like the normal (NO), inner race (IR), outer race (OR), and rolling elements (RE). In this dataset, a fault size of 0.5 mm diameter is taken, and the speed is kept at 1000 rpm. Figures 3 and 4 show the test rig of the two datasets.

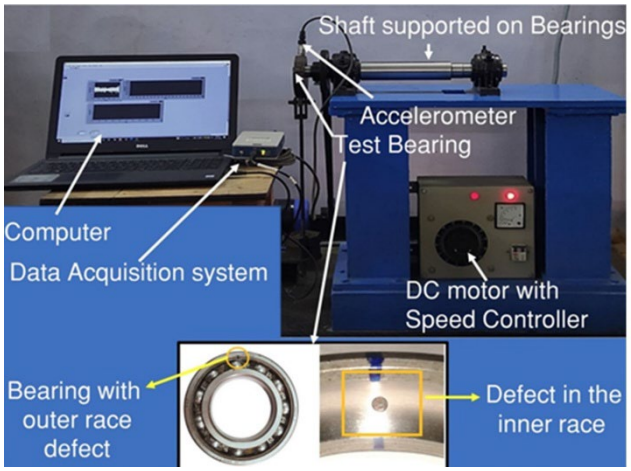

Figure 4. The experimental setup of the test-rig dataset.

4.2 Performance measures

In the context of a fault detection model for rolling bearings, the formulas for accuracy, precision, and recall are based on the outcomes of fault detection predictions. Table 3 shows the expressions considered for measuring performance.

Table 3. Expressions for computing the performance measures.

Measures	Expressions
Accuracy	$\frac{A_{ne}+A_{po}}{A_{ne}+A_{po}+B_{ne}+B_{po}}$
Precision	$\frac{A_{po}}{A_{po}+B_{po}}$
Recall	$\frac{A_{po}}{A_{po}+B_{ne}}$

where $A_{po}$is true Positive (The model correctly identifies a bearing fault when there is a fault); A_{ne} is True Negative (The classifier correctly identifies no fault when there is no fault); $B_{po}$is False Positive (The model incorrectly identifies a bearing fault when there is no fault); $B_{ne}$is False Negative (The model fails to identify a bearing fault when there is a fault).

4.3 Comparative analysis

The following section presents the comparative analysis of various approaches, and it is evaluated using accuracy, precision, and F1 score. The STFT of the denoised VMD signal for the four conditions of bearing and the S-STFT are plotted in Figures 5 to 7. In the STFT, insights into the raw vibration patterns of the rolling bearing signals can be seen along the time axis, while the distribution of signal power across different frequencies can be observed along the frequency axis.

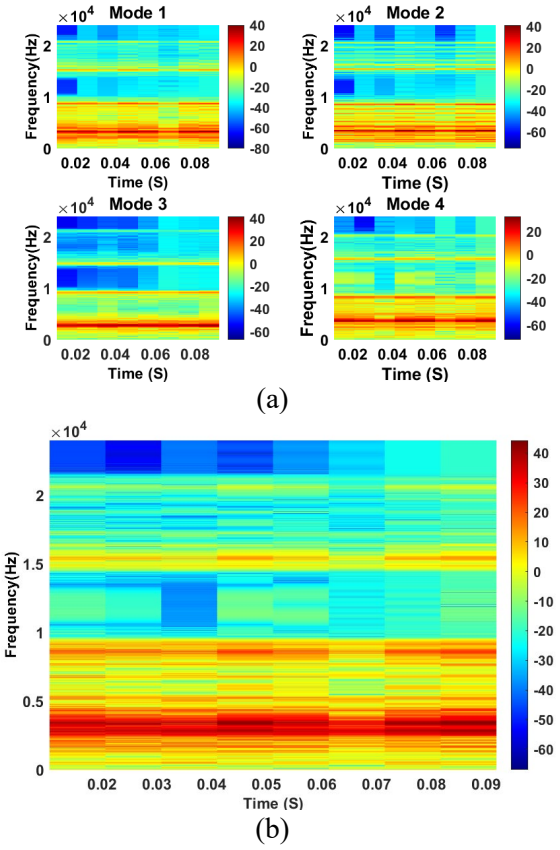

Figure 5. Time - frequency images of (a) STFT and (b) S-STFT of the ball fault.

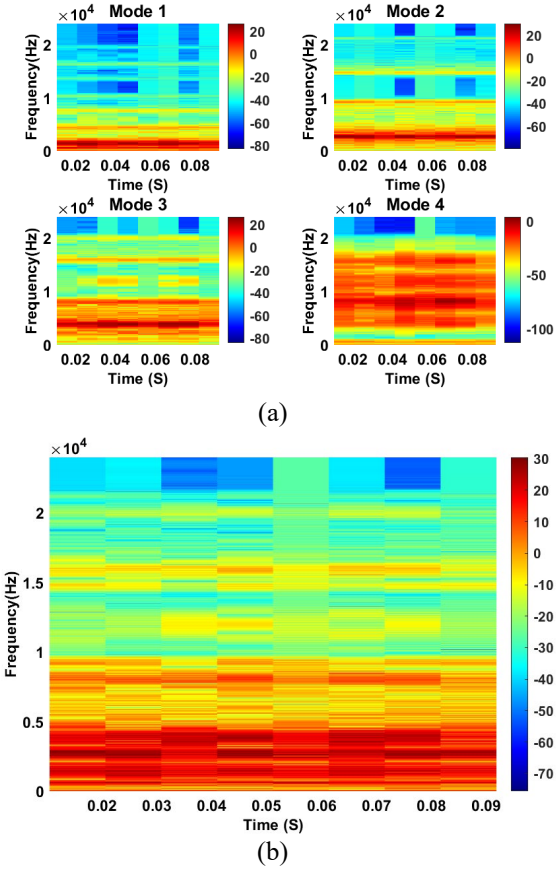

Figure 6. Time-frequency images of (a) STFT and (b) S-STFT of IR.

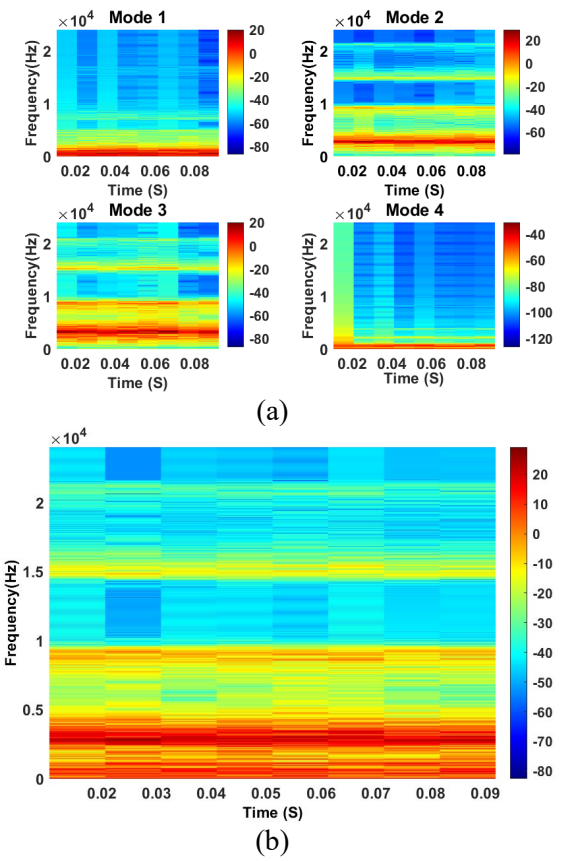

Figure 7. Time-frequency images of (a) STFT and (b) S-STFT of OR.

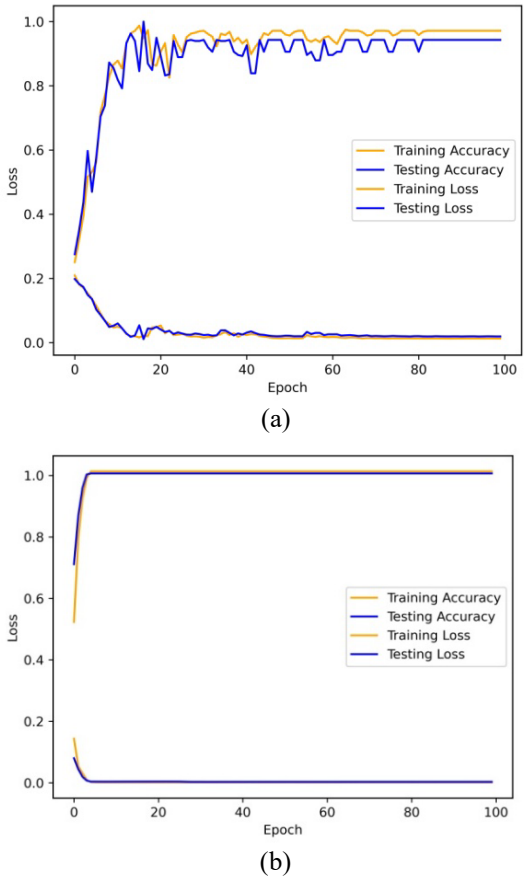

Figure 8. Accuracy-loss curves of the suggested enhanced SqueezeNet model (a) CWRU and (b) Test-rig.

Figure 8 illustrates the accuracy-loss curves of the enhanced SqueezeNet model for the CWRU and test-rig dataset. The training and testing curves show how the enhanced SqueezeNet's accuracy improves or stabilizes over training epochs, while the loss indicates the decrease in error. It is proved that the suggested enhanced SqueezeNet accurately classify detects faults in rolling bearings based on vibration signals. Figure 9 depicts the comparative analysis of the accuracy with respect to the DL models like CNN, ResNet, SqueeezeNet and the proposed enhanced SqueezeNet. It is proved that the accuracy values achieved by the enhanced SqueezeNet are 99.71% (test-rig) and 99.65% (CWRU). These findings proved the effectiveness of the enhanced SqueezeNet model in accurately detecting faults in rolling bearings, outperforming other DL approaches in terms of accuracy among the two datasets.

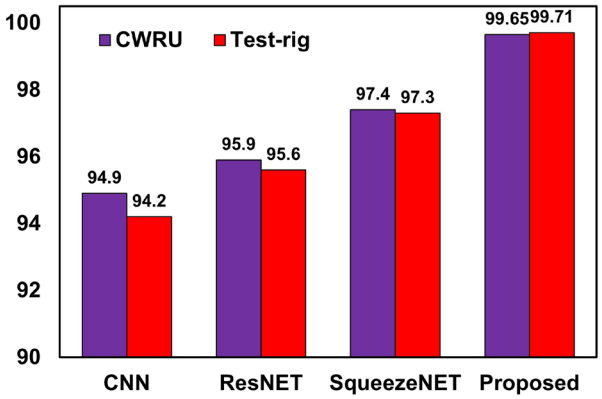

Figure 9. Comparative analysis of the accuracy.

Figure 10 presents a comparative analysis of precision among different DLs, namely CNN, ResNet, SqueezeNet, and the proposed enhanced SqueezeNet. The results validate that the enhanced SqueezeNet achieves precision values of 99.68% on the test-rig dataset and 99.79% on the CWRU dataset. These findings highlight the enhanced SqueezeNet's effectiveness in accurately detecting faults in rolling bearings, showcasing superior performance compared to other DL approaches evaluated on both datasets.

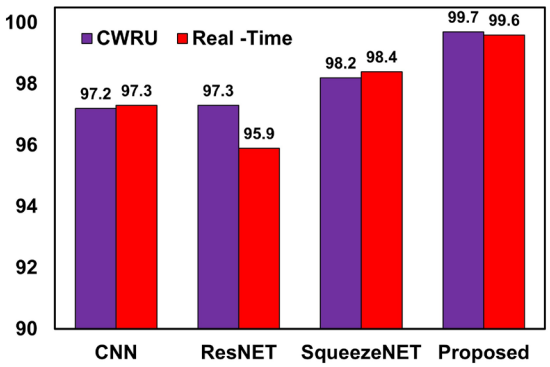

Figure 10. Comparative analysis of precision.

Figure 11 presents a comparative analysis of recall among different DL models. It is observed that the recall values achieved on the CNN are 92.2%, ResNet is 92.9%, SqueezeNet is 95.8%, and the suggested enhanced SqueezeNet is 99.8% on the test-rig dataset. Likewise, recall values achieved by the CNN is 91.9%, ResNet is 92.3%, SqueezeNet is 96.3%, and the suggested enhanced SqueezeNet is 99.6% on the CWRU dataset. In this comparative analysis, the suggested enhanced SqueezeNet attained better outcomes and was efficiently utilized in the fault detection process.

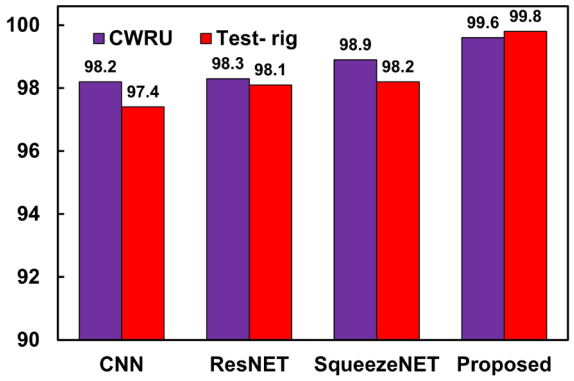

Figure 11. Comparative analysis of the Recall.

Table 4 depicts the comparison with recent works with respect to accuracy. In this comparative analysis, the suggested S-STFT- SqueezeNet-GJA also achieved better accuracies on both datasets.

Table 4. Comparison with recent works.

References	Accuracy (%)
Li et al. [10]	84.2
Yang et al. [11]	99.1
Sun et al. [12]	97.5
Che et al. [13]	99.5
Zhao et al. [14]	98.7
An et al. [15]	99.1
Han et al. [16]	97.5
Niu et al. [17]	98.4
Proposed	99.71 (CWRU) and 99.71 (Experimental)

5. CONCLUSIONS

In this study, a robust fault detection model for rolling bearings is introduced by integrating the GJA with the SqueezeNet with S-STFT of vibration signals as input. The suggested approach employs the efficient architecture of SqueezeNet, optimized by the GJA to enhance its performance in fault detection

tasks. Experimental validation on two different datasets demonstrated that the suggested approach achieved high accuracy, precision, and recall, thereby effectively identifying the faults. This model enhanced the fault detection capabilities and ensured that the model can be deployed in real-time applications with limited computational resources. Overall, the integration of GJA with SqueezeNet provides a better solution for fault detection in rolling bearings and achieves higher accuracy values of 99.71 (CWRU) and 99.71 (test-rig), respectively. The future scope of the work will be in refining the model and exploring its applicability to various kinds of machinery and fault detection scenarios. In addition, this methodology can be focused on improving the robustness of the suggested models to noisy and imbalanced datasets, which are common in real-world fault detection requirements.

REFERENCES

[1] Fan, H.; Xue, C.; Zhang, X.; Cao, X.; Gao, S.; Shao, S., Vibration Images-Driven Fault Diagnosis Based on CNN and Transfer Learning of Rolling Bearing under Strong Noise, *Shock and Vibration*, 2021, pp. 1–16. DOI:10.1155/2021/6616592.

[2] Chang, M.; Yao, D.; Yang, J., Intelligent Fault Diagnosis of Rolling Bearings Using Efficient and Lightweight ResNet Networks Based on an Attention Mechanism, *IEEE Sensors Journal*, 2022, Vol. 23, pp. 9136–45. DOI: 10.1109/JSEN.2023.3251654.

[3] Hoang, D.-T.; Kang, H.-J., Rolling element bearing fault diagnosis using convolutional neural network and vibration image, *Cognitive Systems Research*, 2019, Vol 53, pp. 42–50. DOI: 10.1016/j.cogsys.2018.03.002.

[4] Lu, C.; Wang, Z.; Zhou, B., Intelligent fault diagnosis of rolling bearing using hierarchical convolutional network-based health state classification, *Advanced Engineering Informatics*, 2017, Vol. 32, pp. 139–51. DOI: 10.1016/j.aei.2017.02.005.

[5] Jha, R.K.; Swami, P.D., Fault diagnosis and severity analysis of rolling bearings using vibration image texture enhancement and multiclass support vector machines. *Applied Acoustics*, 2021, Vol. 182, pp. 108243. DOI: 10.1016/j.apacoust.2021.108243.

[6] Qin, Y.; Liu, H.; Mao, Y., Faulty rolling bearing digital twin model and its application in fault diagnosis with imbalanced samples. *Advanced Engineering Informatics*, 2024, Vol. 61, pp. 102513. DOI: 10.1016/j.aei.2024.102513.

[7] Sun, Y.; Li, S.; Wang, X., Bearing fault diagnosis based on EMD and improved Chebyshev distance in SDP image. *Measurement*,2021, Vol. 176, pp. 109100, DOI: 10.1016/j.measurement.2021.109100.

[8] Geng, H.; Peng, Y.; Ye, L.; Guo, Y., Generalized broadband mode decomposition method and its application in fault diagnosis of variable speed spherical roller bearing, *Measuremen*t, 2023, Vol. 208, pp. 112450. DOI: 10.1016/j.measurement.2023.112450.

[9] Hoang, D.T.; Kang, H.J., (2019) Rolling element bearing fault diagnosis using convolutional neural network and vibration image*, Cognitive Systems Research*, 2019, Vol. 53, pp. 42–50. DOI: 10.1016/j.cogsys.2018.03.002.

[10] Vlase, S., Itu, C., Marin, M., Luminta Scutaru, M., Sabou, F. and Necula, R., 2024. Vibration analysis of the Gamma-Ray element in the ELI-NP interaction chamber (IC). Journal of Computational Applied Mechanics, 55(2), pp.275-288.

[11] Ma J, Wu J, Wang X. Fault diagnosis of rolling bearing based on TKEO-ELM. UPB Sci. Bull., Series D. 2017; 79(4), 215-26.

[12] WU Z, LIU Y, LI X, Du X, Wang B. Intelligent fault diagnosis of robot bearing based on multi-information. UPB Scientific Bulletin, Series D: Mechanical Engineering. 2020; 82(3), 145-235.

[13] Li, X.; Jiang, H.; Wang, R.; Niu, M., Rolling bearing fault diagnosis using optimal ensemble deep transfer network, Knowledge-*Based Systems*, 2021, Vol. 213, pp. 106695. DOI: 10.1016/j.knosys.2020.106695.

[14] Yang, X.; Liu, B.; Xiang, L.; Hu, A.; Xu, Y., A novel intelligent fault diagnosis method of rolling bearings with small samples, *Measurement*, 2022, Vol. 203, pp. 111899. DOI: 10.1016/j.measurement.2022.111899.

[15] Sun, Y.; Li, S.; Wang, Y.; Wang, X., Fault diagnosis of rolling bearing based on empirical mode decomposition and improved manhattan distance in symmetrized dot pattern image, *Mechanical Systems and Signal Processing*, 2021, Vol. 159, pp. 107817. DOI: 10.1016/j.ymssp.2021.107817.

[16] Che, C.; Wang, H.; Ni, X.; Lin, R., Hybrid multimodal fusion with deep learning for rolling bearing fault diagnosis, *Measurement*, 2021, Vol. 173, pp. 108655. DOI: 10.1016/j.measurement.2020.108655

[17] Zhao, J.; Yang, S.; Li, Q.; Liu, Y.; Gu, X.; Liu, W., A new bearing fault diagnosis method based on signal-to-image mapping and convolutional neural network, *Measurement*, 2021, Vol. 176, pp. 109088. DOI: 10.1016/j.measurement.2021.109088.

[18] An, F.; Wang, J., Rolling bearing fault diagnosis algorithm using overlapping group sparse-deep complex convolutional neural network, *Nonlinear Dynamics*, 2022, Vol. 108, pp. 2353–68, DOI: 10.1007/s11071-022-07314-9.

[19] Han, M.; Wu, Y.; Wang, Y.; Liu, W., Roller bearing fault diagnosis based on LMD and multi-scale symbolic dynamic information entropy, *Journal of Mechanical Science and Technology*, 2021, Vol. 35, pp. 1993–2005. DOI: 10.1007/s12206-021-0417-3.

[20] Niu, G.; Wang, X.; Golda, M.; Mastro, S; Zhang, B., An optimized adaptive PReLU-DBN for rolling element bearing fault diagnosis, *Neurocomputing*, 2021, Vol. 445, pp. 26–34. DOI: 10.1016/j.neucom.2021.02.078.

[21] Nicodim M, Gheorghiu H. Identification of faults rolling bearings through vibration and shock impulses analysis. UPB Sci. Bull., Series D. 2011;73(1):63-70.

[22] Koonce B, Koonce B. SqueezeNet. Convolutional neural networks with swift for tensorflow: image recognition and dataset categorization. 2021:73-85.

[23] Zhang, J.; Duan, L.; Luo, S.; Li, K., Fault diagnosis of reciprocating machinery based on improved MEEMD-SqueezeNet, Measurement, 2023, Vol. 217, pp. 113026. DOI: 10.1016/j.measurement.2023.113026.

[24] Case Western Reserve University Bearing Data Center Website http://csegroups.case.edu/bearingdatacenter/home